Relaxation of stresses in glass surface regions by subcritical crack growth

T. Fett, K.G. Schell, C. Bucharsky, G. Rizzi

IAM Institute for Applied Materials

Impressum

Karlsruher Institut für Technologie (KIT)
www.kit.edu

Abstract

In previous reports, we dealt with the SIF computations of semi-elliptical surface cracks introduced in glass specimens by grinding. It can simply be shown that subcritical extension of such cracks must result in a reduction of stresses applied to the specimen.

We apply this effect on tensile tests and on torsion tests by Aaldenberg et al. carried out on cylindrical specimens at temperatures between 550°C and 700°C in normal lab air environment. The torsion moments M_t measured by Aaldenberg et al. decreased with time t for a constant drill angle. This effect was interpreted by Aaldenberg et al. as a proof for a relaxation effect by the presence of molecular water.

In the present report, we discuss the possibility that the reduction of the torsion moment is caused by subcritical crack growth that results in comparable effects.

Contents

1. Local stress intensity factors

Cracks generated on glass surfaces during machining are responsible for strength and lifetimes of mechanically loaded specimens. The same holds for artificially introduced indentation cracks. The semi-elliptical cross section of such a surface crack is shown schematically in Fig. 1a. The crack depth is denoted as a and crack width as $2c$. The parametric angle along the crack front is φ and the stress acting normal on the crack plane is σ. The deepest point of the crack is generally denoted as point (A) and the intersection points at the surface as (B).

For the computation of local stress intensity factors $K(\varphi)$ under a tensile stress σ, the well established relation of Newman and Raju [1] may be used. This relation reads

$$K = \sigma Y \sqrt{a} \tag{1}$$

with the geometric function Y modified in [2] and plotted in Fig. 1b versus the parametric angle φ for different aspect ratios a/c. For aspect ratios of $a/c<0.826$, the stress intensity factor is at (A) higher than at points (B). At $a/c>0.826$, the reverse applies, $K_A<K_B$. For the special case of $a/c=0.826$ the stress intensity factors at the surface and the deepest point are identical as indicated by the squares.

In preceding reports [2,3] we dealt with the determination of stress intensity factors for semi-elliptical surface cracks caused by surface treatments like grinding. These derivations were based on the solution by Newman and Raju [1].
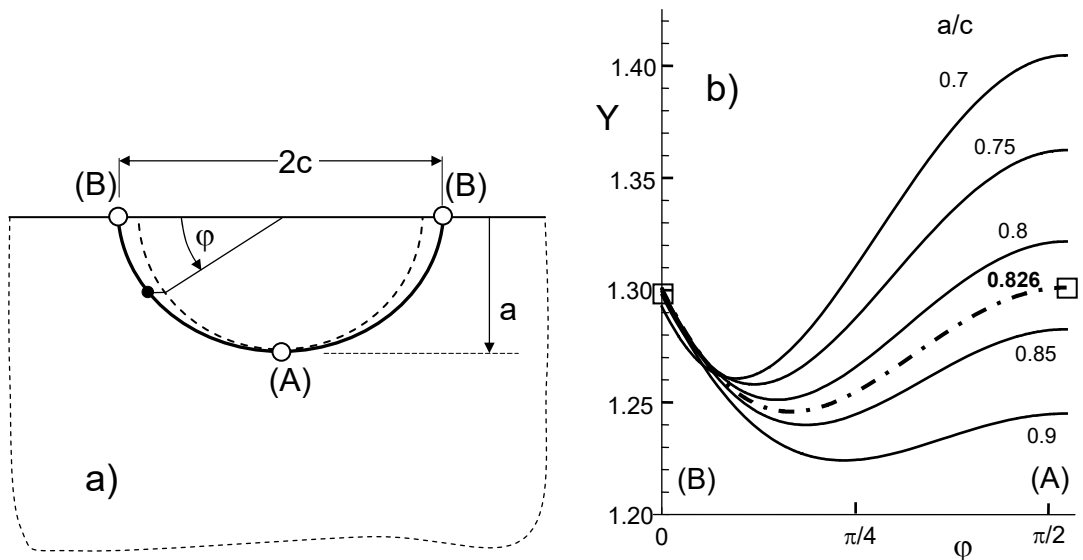

Fig. 1 a) Geometry of a semi-elliptical surface crack normal to the applied stress, b) geometric function along the crack front for several aspect ratios a/c, dash-dotted line: curve for which $Y_A=Y_B$ (represented by squares).

1

Figure 1b implies that:

- There exists no aspect ratio for a semi-ellipse that yields a constant stress intensity factor along the crack front.

- Even for the aspect ratio of a/c=0.826 for which the local stress intensity factors at the surface and the deepest point of the semi-ellipse are identical, the stress intensity factor shows a significant variation with the angle φ. This fact causes problems in describing crack propagation. Problems are obvious even in the simplest case of crack extension, namely, stable crack growth at $K=K_{Ic}$. By load application to a semi-elliptic crack of a/c=0.826, the critical stress intensity factor is at first reached at the surface and the deepest points. These regions can extend but the regions at which $K(\varphi) < K(0°,90°)$ must stay behind a semi-ellipse (Fig. 2). Already after the first infinitesimally small step of crack extension, the crack geometry must deviate from a semi-ellipse and, consequently, the semi-ellipse solution can no longer be applied to this now slightly irregular crack shape. This makes evident that stable and subcritical crack growth prediction on the basis of local stress intensity factors is not simply possible. From observation of the crack shape during stable and fatigue crack propagation it could be concluded that cracks propagated as semi-ellipses although local stress intensity factors did not allow this. An irregular shape to be expected from the local variation of the stress intensity factors was not detectable. A way out of this dilemma was proposed very early by Cruse and Besuner [4].
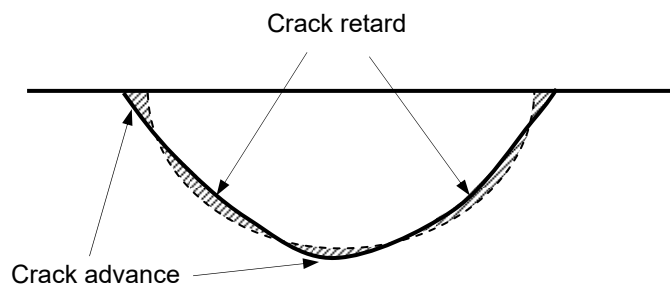

Fig. 2 Prediction of a semi-elliptical crack extension by stable or subcritical crack propagation, schematic, dashed front: original crack, solid front: Front, developed during crack propagation.

2 Averaged stress intensity factors according to Cruse and Besuner

A simple fracture mechanics tool to compute the shape of semi-elliptical surface cracks is the computation of so-called averaged stress intensity factors. The definition of the average stress intensity factor $\overline{K}$ according to Cruse and Besuner [4,5] is

$$\overline{K} = \sqrt{\frac{1}{\Delta S} \int\limits_{(\Delta S)} K^2 d(\Delta S)} \qquad (2)$$

Two independent virtual crack changes that preserve the semi-elliptical crack shape were proposed by Cruse and Besuner [4], namely, crack depth increment Δa with width c kept constant

$$\Delta S_A = \frac{1}{2}\pi c \Delta a \ , \ d(\Delta S_A) = c\Delta a \sin^2 \varphi \, d\varphi \qquad (3)$$

or crack width increment Δc with depth $a = \text{const}$

$$\Delta S_B = \frac{1}{2}\pi a \Delta c \ , \ d(\Delta S_B) = a\Delta c \cos^2 \varphi \, d\varphi \qquad (4)$$

as illustrated in Fig. 3 by the hatched areas.

It should be emphasized that the Cruse-Besuner approach for the computation of averaged stress intensity factors was examined intensively in the eighties and early nineties. Only a few papers may be mentioned in this context which shows that the method is applicable to various types of cracks (for references see [3]).

The use of this type of stress intensity factors allowed very good predictions for the development of the crack shape in tension and bending and correct predictions of crack growth rates in fatigue tests. In the following considerations stress intensity factors defined by eqs.(2) to (4) will be addressed.
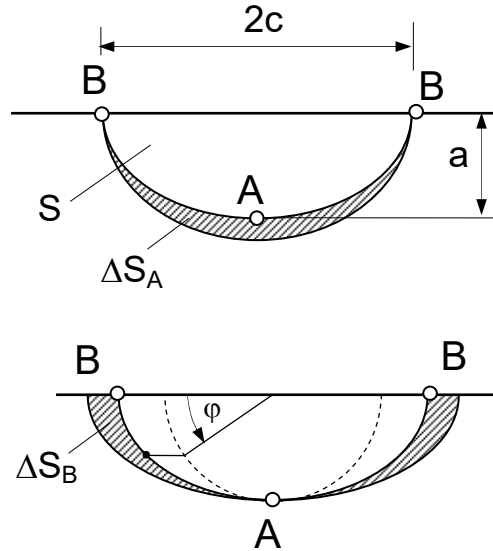

Fig. 3 Virtual crack extensions according to Cruse and Besuner [4].

The virtual crack extensions according to (3) and (4) resulted in the averaged stress intensity factors of Fig. 4.

By curve fitting, we obtained approximate relations for the averaged geometric functions at points (A) and (B) defined by

$$\overline{K}_{A,B} = \sigma \overline{Y}_{A,B} \sqrt{a} \qquad (5)$$

Particularly noteworthy is the fact that in the range $0.75 < a/c < 3$ the stress intensity factor $\overline{K}_A$ is almost constant (indicated by the dash-dotted horizontal line in Fig. 4a). Therefore, it can be written

$$\overline{K}_A = \sigma \, 1.17\sqrt{c} \qquad (6)$$

The curves of the K-factors defined according to eq.(2) intersect at about $a/c \approx 0.85$. For aspect ratios of $a/c < 0.85$, the averaged stress intensity factor is at (A) higher than at points (B).
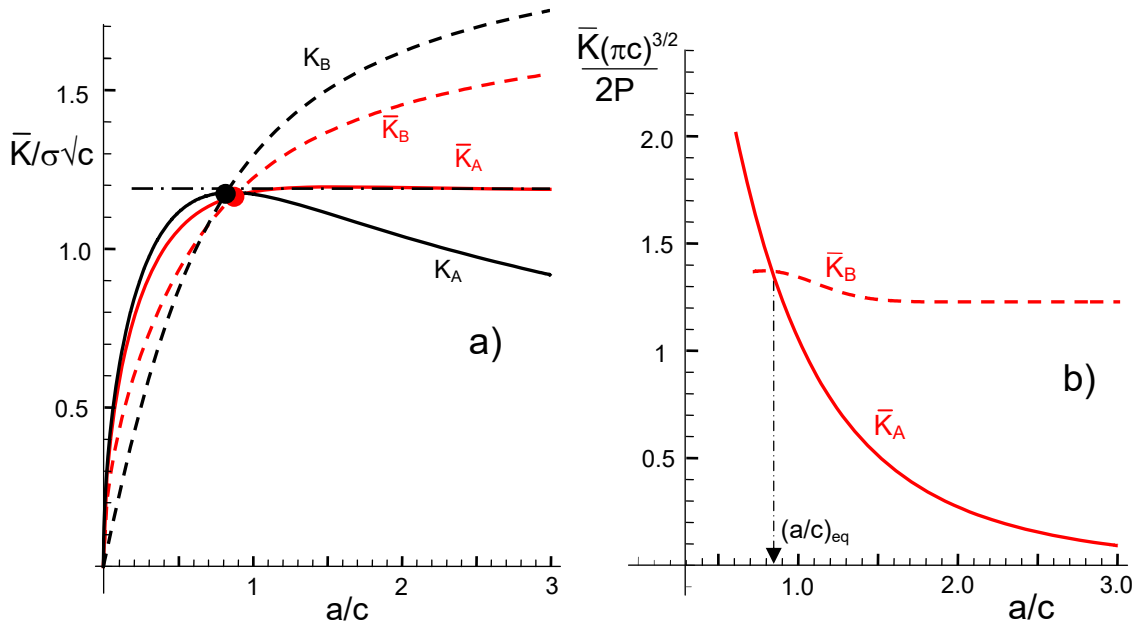

Fig. 4 a) Local and averaged stress intensity factors for constant stresses over the crack area normalized on crack width c [2,3], b) averaged stress intensity factors for loading by concentrated forces at the surface [3], arrow: equilibrium aspect ratio $(a/c)_{eq} \cong 0.84$.

3. Surface cracks under concentrated forces

Figure 5 shows a crack that has been created under a strongly localized contact between a grain of a grinding wheel and the glass surface.

The result of such a contact may be described by a crack-like damage similar to the cracks obtained by Vickers indentation tests. Beneath the contact area of indenter and glass surface, a residual stress zone of depth ρ remains even after unloading. Plastically deformed glass and material pressed between the crack flanks act as a wedge and open the crack. The result is a positive stress intensity factor $K_r > 0$. If the size of the

residually stressed zone is sufficiently small compared to the crack size, the stresses distributed over a cross-section of radius ρ, may be replaced by a single point force P at the crack mouth that acts perpendicularly on the crack plane. The stress intensity factors for such a crack-face loading were fitted in [2].
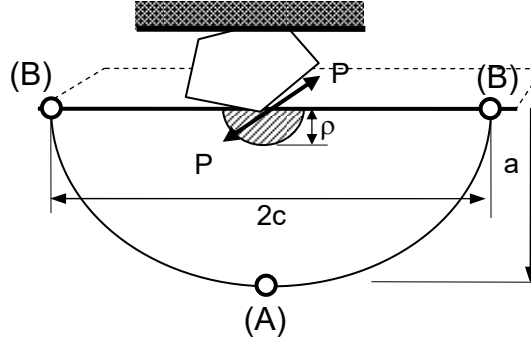

Fig. 5 Geometric data of an indentation crack: Indentation process by a single grain of the grinding wheel, resulting in a semi-elliptical surface crack of depth a and width $2c$.

Averaged stress intensity factors for the semi-elliptical crack under a point force are available in Chapter F4.2 of [6]. These results are plotted in Fig. 6a for the limited range of $0.7 \leq a/c \leq 1$ expressed in [6] by

$$\overline{K}_{A,B} = \frac{2P_{semi}}{(\pi a)^{3/2}} \overline{F}_{A,B} = \frac{2P_{semi}}{(\pi c)^{3/2}} \left(\frac{c}{a}\right)^{3/2} \overline{F}_{A,B} \tag{7}$$

Numerical results for local stress intensity factors on embedded elliptical cracks subjected by point forces were reported by Atroshchenko [7] in Figs. 3.16 and 3.18.
As approximate relations for the averaged stress intensity factors we suggest in [3] for the extended region $0.7 \leq a/c \leq 3$.

$$\overline{K}_A \frac{(\pi c)^{3/2}}{2P_{semi}} \cong \frac{3.74}{\dfrac{a}{c} + \left(\dfrac{a}{c}\right)^2 + \left(\dfrac{a}{c}\right)^3} \left(1 - \exp\left[-1.76\frac{a}{c}\right]\right) \tag{8}$$

for point (A), and

$$\overline{K}_B \frac{(\pi c)^{3/2}}{2P_{semi}} \cong 1.22 + 0.144 \exp\left[-5.06\left(\frac{a}{c} - 0.775\right)^2\right] \tag{9}$$

for point (B), both solutions introduced in Fig. 4b.
Here we consider surface cracks in the half-space in order to be able to neglect geometry-related influences on the K-factors.

4. Growth of cracks pinned at the surface

4.1 Model for pinned cracks

In ground silica surfaces many cracks are present even in the case of finishing by mechanical polishing or chemical etching. This has been outlined by Suratwala et al. [8]. The individual distributions of the depths and the widths are approximated in [8] by exponential distribution functions. Since there are many surface cracks present on the surface, crack interaction must occur during crack propagation, e.g. during subcritical crack growth in humid environment under stress σ. This is schematically illustrated by Fig. 6a, where the considered crack terminates on two other cracks. The considered crack is "pinned" with respect to propagation along the surface. In order to avoid restrictions on the extent of the crack (for example by back-wall effects) and the associated more complicated calculations, reference should be made here to the case of the half-space.
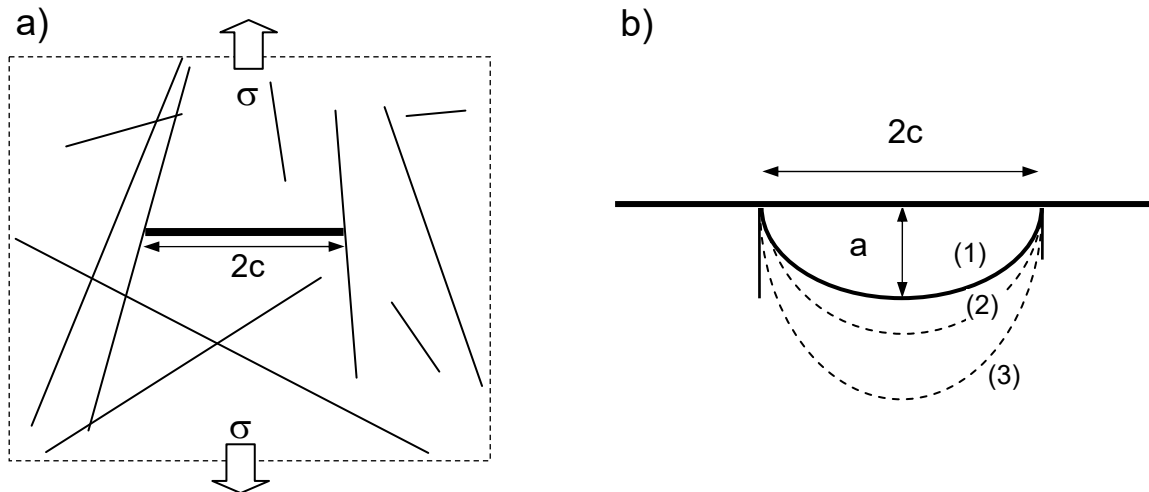

Fig. 6 a) Semi-elliptical crack pinned at the surface, b) crack front development during crack growth.

After the grinding treatment, the glass surfaces can be in different states. In most cases, the machined samples are subjected to an annealing treatment in order to eliminate internal stresses that have been introduced. In this case, the total stress intensity factor K_{total} consists on the effect of externally applied loading by σ_{appl} exclusively, i.e.

$$K_{total,A} = K_{appl,A} \qquad (10)$$

This $K_A(a)$-dependency is plotted in Fig. 7 as the red line.

Without an annealing treatment, the wedging of splitting forces P generated by the indentation processes remain active. In this case, the total stress intensity factor $K_{total,A}$ $=K_A$ (magenta) is given by superposition of the applied stress intensity factor (red) and the indentation stress intensity (blue)

$$K_{total,A} = K_{appl,A} + K_{indent,A} \qquad (11)$$

Since the indentation term decreases continuously with increasing crack depth a, the solution eq.(11) approaches asymptotically the straight line eq.(10). The individual stress intensity factors by eqs.(10) and (11) are plotted in Fig. 7 normalized on fracture toughness K_{Ic}.

The main difference to the normal crack behavior, in which all specimens were annealed sufficiently high and long stress-free, is the fact that after grinding, the stress intensity factor directly after introduction, $t \rightarrow 0$, is almost equal to the fracture toughness even in the absence of external loading. The consequence of any crack growth is a decrease of the total stress intensity factor K_A.
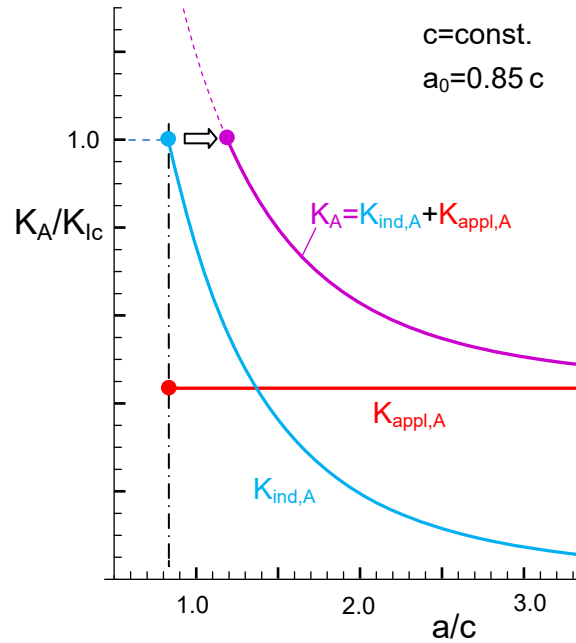

Fig. 7 Total stress intensity factors K_A subsuming contributions of splitting forces $K_{ind,A}$ and external loading $K_{appl,A}$. Arrow indicates spontaneous depth extension after external load application.

4.2 Annealed specimen

Since no detailed information is given by Aaldenberg et al. [13] on the surface state (roughness, crack density, strength for the different surface states, occurrence of possible delayed fracture during the tests) it doesn't make any sense to perform quantitative computations. Therefore, we will show the expected effect by qualitative analysis on the basis of well-known fracture mechanical relationships.

In most cases, the machined samples are subjected to an annealing treatment in order to eliminate internal stresses that have been introduced.

A crack pinned at the surface can be described by a constant width c=const. This implies for constant stress intensity factors according to (6) a constant subcritical crack growth rate, i.e.

$$\overline{K}_A = \sigma\, 1.17\sqrt{c} = \text{const.} \Rightarrow v = \frac{da}{dt} = \text{const.} \tag{12}$$

A constant crack extension rate is equivalent to a crack depth proportional to the time

$$v = \frac{da}{dt} = \text{const.} \Rightarrow \Delta a = a - a_0 \propto t \tag{13}$$

(a_0=initial crack depth).

The energy release rate G for a crack surface increment dS under a load F is given by the increase of the compliance C according to

$$G = \frac{F^2}{2}\frac{dC}{dS}\,. \tag{14}$$

On the other hand, the energy release rate G and the stress intensity factor K are inter-related by

$$G = \frac{K^2}{E'} \tag{15}$$

where E' is the plain-strain Young's modulus $E'=E/(1-v^2)$.

Since c=const. the crack-area increment dS can be replaced by the crack depth increment da. Consequently, eqs.(13-15) give

$$\frac{dC}{da} \propto K_A^2 \Rightarrow \frac{dC}{da} = \text{const.} \Rightarrow \Delta C \propto \Delta a \Rightarrow \Delta C \propto t \tag{16}$$

Since the compliance C is increased, we can conclude that the surface region in which the crack is located becomes more compliant. The effective Young's modulus seems to be reduced in the surface region (although the physical module remains unchanged). In a cylindrical specimen, the surface layer undergoes the same strains and displacements than the bulk material. Under such constant displacement conditions the increase of the compliance in the crack-affected surface layer must cause there a decrease of stresses $\Delta\sigma$ in tensile tests. Consequently, the stresses in the surface layer are less than in the bulk:

$$\Delta C \propto t \quad \Rightarrow \Delta\sigma \propto t \tag{17}$$

Finally, the decrease of the tensile stresses results in a decrease of the total load

$$\Delta\sigma \propto t \quad \Rightarrow \Delta P \propto \Delta\sigma \propto t \tag{18}$$

4.3 Subcritical crack growth at 700°C

For the computation of the crack depths a as a function of time, one can use the subcritical crack growth data measured by Aaldenberg and Lezzi [9] as plotted in Fig. 8 for 700°C in lab air. We fitted their data (circles) by an equation that was suggested in literature (see [10])

$$v = \frac{da}{dt} = \begin{cases} 0 & \text{for } K < K_0 \\ A \, \sinh[B(K - K_0)] & \text{for } K \geq K_0 \end{cases} \tag{19}$$

with the parameters $A = 4 \times 10^{-9}$ m/s, $B = 46.8$/MPa√m, $K_0 = 0.53$ MPa√m. This dependency is shown in Fig. 8 by the solid line. In a linear description on the basis of chemical reaction theory [11,12], the well-known $v(K)$-relation reads

$$v = \frac{da}{dt} = A \exp[BK] \tag{20}$$

given by the red line in Fig. 8 with a deviating value of A=6.9 10^{-20} m/s.
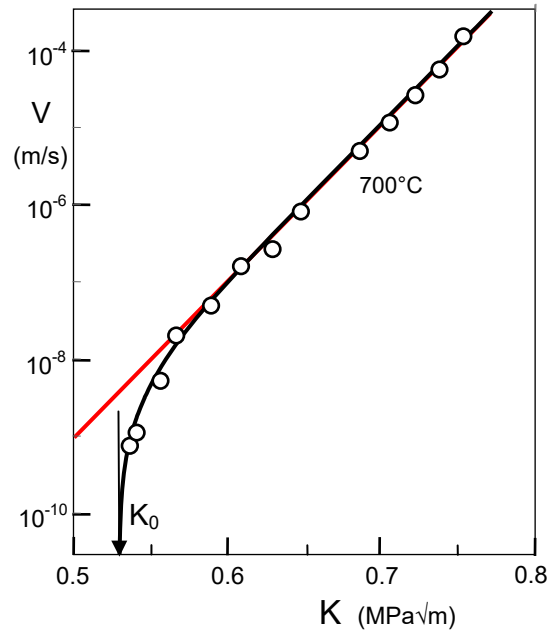

Fig. 8 Subcritical crack growth of silica in humid air at 700°C: Circles: measured by Aaldenberg and Lezzi [9], red line: eq.(20), black curve: eq.(19).

4.4 Change of crack depth, compliance and load bearing capacity

Computation of crack growing via eqs.(11) and (19) was performed for the assumed data: c=const.=200 µm, a_0=0.85 c, K_0=0.53 MPa√m, K_{Ic}=0.75 MPa√m. In order to keep the calculations as clear as possible, it is assumed that inert conditions may exist during surface treatment and storage. The influence of moisture should start at the same time as the mechanical load. The time-dependent increases in crack length, Δa,

9

compliance ΔC, and load-bearing capacity, ΔF, are shown in Fig. 9a by the black curves. The parameters at the curves represent the ratio of applied to threshold stress intensity factor, K_{appl}/K_0. The red curves would result from eq.(20), i.e. in the absence of a threshold stress intensity. Figure 9b illustrates again the curve for $K_{appl}/K_0=1.025$ in Fig. 9a. In addition, the asymptote for $t\to\infty$ is shown as a dash-dotted straight line and the result for annealed samples with $K_{ind}=0$ as a dashed straight line.
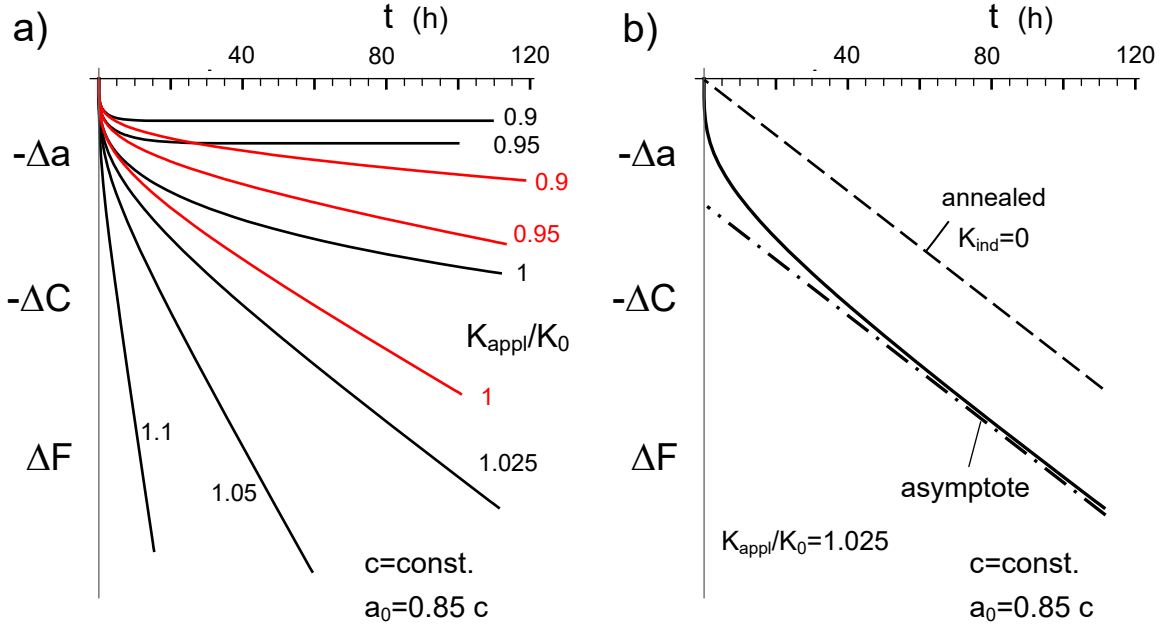

Fig. 9 a) Change of crack depth Δa, compliance ΔC and load-bearing capacity ΔF vs. time t. Computed for c=const.=200 µm, a_0=0.85 c, K_0=0.53 MPa√m, K_{Ic}=0.75 MPa√m, b) dash-dotted straight line indicates the asymptote to the curve for $K_{appl}/K_0=1.025$, dashed line represents the case of annealed specimen with $K_{ind}=0$.

5. Application to torsion measurements

In our opinion, the increase of the compliance could also be the reason for the "relaxation effect" observed in the experiments by Aaldenberg et al. [13], where torsion tests on silica cylinders were performed at temperatures between 550°C and 700°C in normal lab air environment. The torsion moments M_t were measured as a function of time t for a constant drill angle as plotted in Fig. 10. Different surface states were reached by grinding, polishing and flame-polishing. The results are plotted in the form

$$\Delta M_t(t) = M_t(t) - M_0 \tag{21}$$

vs $\sqrt{t}$, where M_0 is the moment at t=0. This report deals with the question of the fundamental effect of silica swelling by hydroxyl generation on twisted cylinder samples. In this study, two effects will be discussed qualitatively.

The results for the uniaxial loading case may be used to describe more complicated loading by superposition. Under torsion loading, the maximum and minimum principle stresses appear in a coordinate system turned by 45° with respect to the length axis. In this system, the "applied" stresses are

$$\sigma_{appl,y} = -\sigma_{appl,z} \tag{22}$$

which fulfil simply $\tau_{appl}=(\sigma_{y,appl}+\sigma_{x,appl})/2=\sigma_{y,appl}$.

In a statistical sense, half of the surface cracks are normal to the tensile and half normal to compressive stresses. Trivially, the cracks under compression cannot undergo any subcritical crack growth. From the cracks normal to tension, it has to be expected that under torsion loading a relation for the torque must hold equivalent to (18):

$$\Delta\tau \propto t \quad \Rightarrow \Delta M_t \propto \Delta\tau \propto t \tag{23}$$

The straight lines in Fig. 10 indicate the asymptotically reached linear dependency of $\Delta M_t \propto t$ in (23), the deviations for short times t, i.e. small crack extensions Δt, reflect the fact that in the "short-extension region" the indentation stress intensity factor K_{ind} contributes maximum to the total stress intensity factor via eq.(11). Depending on the v-K-curve, the higher K_{total} must result in clearly increased crack-growth rates $v=da/dt$, compared with the asymptotically approached $K_{total} \rightarrow K_{appl}$.
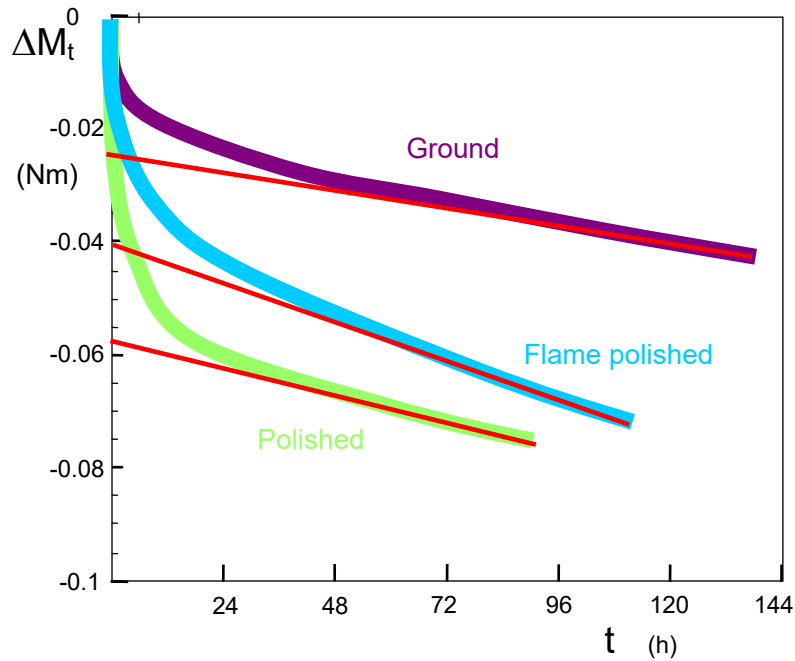

Fig. 10 Change of the torsion moment ΔM for cylindrical silica specimens at 700°C under the condition of constant drill deformations measured by Aldenberg et al. [13].

6. Outlook on future work

The considerations made here are still approximate for the time being. In a further investigation, the influence of interactions between the many cracks in the machined sample surface will be taken into account. Suratwala et al. [8] showed that the size distribution of the individual machining cracks continuously decreases with crack depth up to an upper limit depth a_{max}. Figure 11 shows the crack distribution for several surface treatments in a normalized representation (for details of surface machining see [8]). Of particular importance here is the fact that the depth dimensions of the machining-induced cracks have rather sharp upper limit values a_{max}.

For a quantitative analysis the contributions of the different individual cracks must be superimposed according to the frequency of their occurrence. The feedback of the globally increased compliance on the load of individual cracks is currently being studied.
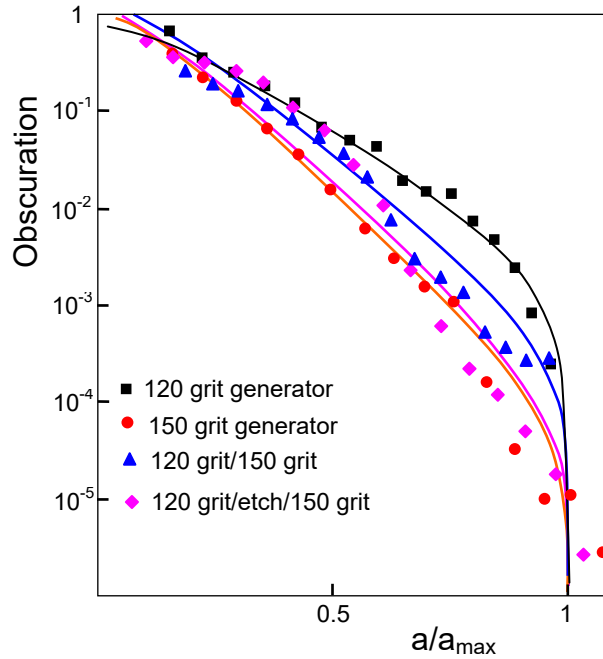

Fig. 11 Measured crack depths after different grinding treatments from [8] in normalized representation.

Another complication is the indentation stress intensity factor present in the mechanical tests. In the unannealed specimens, the initial indentation stress intensity factor $K_{ind,0}$ is not completely retained and lies between the two limit cases of the value directly after the formation of a crack during grinding and the case of the annealed specimen with completely absent $K_{ind} = 0$, i.e. it is in general $0 \leq K_{ind} \leq K_{ind,0}$. The reason for this is the fact that in humid air the indentation cracks can grow subcritically before the mechanical tests are performed.

However, the occurrence of significant subcritical crack propagation is assured. The authors of [13] note that the cylinder specimens failed after some time under the load initially targeted. Unfortunately, there is no mention of how high this tension was. Consequently, an alternative interpretation as a result of subcritical crack growth cannot simply be dismissed out of hand.

References

1 Newman, J.C., Raju, I.S., An empirical stress intensity factor equation for the surface crack, Engng. Fract. Mech. **15**(1981) 185-192.

2 T. Fett, K.G. Schell, C. Bucharsky, Indentation events during surface machining – Compilation of local stress intensity factors, Scientific Working Papers **163**, 2021, ISSN: 2194-1629, Karlsruhe, KIT

3 K.G. Schell, C. Bucharsky, G. Rizzi, T. Fett , Averaged stress intensity factors for semi-elliptical surface cracks, Scientific Working Papers **169**, 2021, ISSN: 2194-1629, Karlsruhe, KIT.

4 Cruse, T.A., Besuner, P.M., Residual life prediction for surface cracks in complex structural details, J. of Aircraft **12**(1975), 369-375.

5 Fett, C. Mattheck, D. Munz, On the accuracy of the Cruse-Besuner weight function approximation for semi-elliptical surface cracks, Int. Journ. of Fracture 40(1989),307-313

6 T. Fett, Stress Intensity Factors, T-Stresses, Weight Functions, Supplement Volume, IKM **55**, KIT Scientific Publishing, 2009.

7 E. Atroshchenko, Stress intensity factors for elliptical and semi-elliptical cracks subjected to an arbitrary mode I loading, Thesis, 2010, University of Waterloo, Ontario, Canada.

8 T. Suratwala, L. Wong, P. Miller, M.D. Feit, J. Menapace, R. Steele, P. Davis, D. Walmer, Sub-surface mechanical damage distributions during grinding of fused silica, J. Non-Cryst. Solids, **352**(2006), 5601-5617.

9 J.S. Aaldenberg, P.J. Lezzi, Measurement of the silica glass fatigue limit, J. Amer. Ceram. Soc. (2020), DOI 10.1111 jace.16970.

10 Fuller, E.R., Thomson, R.M., Lattice theories of fracture, in: Fracture Mechanics of Ceramics Vol. IV (1978), Plenum Press, New York, 507–548.

11 S.M. Wiederhorn and L.H. Bolz, "Stress Corrosion and Static Fatigue of Glass," *J. Am. Ceram. Soc.* **53**[1810], 543-548 (1970).

12 S.M. Wiederhorn, E.R. Fuller, R. Thomson, Micromechanisms of crack growth in ceramics and glasses in corrosive environments, Metal Science, Aug-Sept (1980), 450-458.

13 Aaldenberg EM, Aaldenberg JS, Blanchet TA, Tomozawa M. Surface shear stress relaxation of silica glass. J Am Ceram Soc. 2019;00:1-10. https:doi.org/10.1111/jace.16342